View metadata, citation and similar papers at core.ac.uk

brought to you by CORE

provided by Institutional Repository of the Freie Universität Berlin

Chemistry–A European Journal | doi.org/10.1002/chem.202000881

Check for updates

Nickel Fluorides | *Hot Paper*

Combining Theory and Experiment to Characterize the Voltammetric Behavior of Nickel Anodes in the Simons Process

Stefan Mattsson,*[a] Gene Senges,[b] Sebastian Riedel,[b] and Beate Paulus[a]

Abstract: The Simons process, otherwise known as the electrochemical fluorination (ECF) method, is widely used in industry to electrolytically synthesize chemicals for various purposes. Even to this day, the exact mechanism of the ECF reaction remains unknown, but is believed to involve the formation of an anodic nickel fluoride film with highly oxidized nickel centers. In this study, experiments and density functional theory calculations are combined to characterize the initial anodic peak occurring at potentials typically required in an ECF cell. NiF_2 is believed to form a passivating layer at low potentials. The calculations show that a potential of +3.1 V is required to oxidize surface Ni^{2+} centers to Ni^{3+}. This is in good agreement with the measured anodic peak at +3.57 V.

Introduction

The Simons process is a widely used electrochemical fluorination method (often and herein simply referred to as ECF) for the synthesis of partially or perfluorinated organic compounds such as perfluorobutane sulfonic acid or triflic acid.[1–5] Perfluorinated compounds are widely used as surfactants as well as in soil and stain-resistant coatings.[3,5–10] The fluorination is facilitated on anodically polarized nickel electrodes in anhydrous hydrogen fluoride (aHF).[1,2,11] The process usually runs at current densities lower than 3.0 A dm^{-2} and cell voltages of 4.5 to 6.0 V whilst maintaining the temperature in the range from 0 to 15 °C.[1] Ever since its discovery in the 1940s by Joseph H. Simons,[12–17] the mechanism of the Simons-type ECF has been the subject of controversial debate. Two possible pathways have been considered: the direct electrochemical oxidation and subsequent fluorination of the organic molecule (EC_bEC_N mechanism)[3,18–23] and the electrochemical generation of an oxidizing and fluorinating agent such as fluorine (molecular or radical) or highly reactive nickel fluorides such as NiF_3 (NiF_4).[1,2,24–27]

The EC_bEC_N mechanism (Scheme 1) was introduced by Rozhkov in 1976.[20,22] Rozhkov drew his conclusion from experiments using Pt electrodes and aprotic solvents without considering the actual conditions of the Simons-type ECF (see above).[3,18,19,22,23] The competition between perfluorination and desorption from the electrode surface causes partial fluorination.[18]

$$CH_3SO_2F \xrightarrow[(E)]{-e^-} [CH_3SO_2F]^{+\cdot} \xrightarrow[(C_b)]{-H^+} \dot{C}H_2SO_2F \xrightarrow[(E)]{-e^-} {}^{+}CH_2SO_2F \xrightarrow[(C_N)]{+F^-} CH_2FSO_2F$$

Scheme 1. Schematic of the hypothetical EC_bEC_N mechanism.

In the Simons process, Ni anodes are used in aHF rather than Pt anodes in an aprotic solvent.[1,13–17] Under these conditions, it was suggested that oxidizing Ni agents such as NiF_3 or NiF_4 were formed electrochemically prior to the electrochemical fluorination of the organic substrate.[1,2,28,29] This assumption was supported in 1995 when Sartori, Ignat'ev, and Datsenko experimentally proved that oxidation of *N*,*N*-dimethyltrifluoromethane-sulfonamide occurs on previously polarized Ni anodes, even after disconnection of the cell from the power supply.[28] In addition, in 1997, Bartlett et al. showed that both the Simons-type ECF and the treatment of acetonitrile with R-NiF_3 lead to similar products.[29,30] In 2003, Ignat'ev and Willner reported a black film on the Ni anode during the electrochemical fluorination, which was observed to decompose quickly when exposed to air. This film was believed to be solid, black NiF_3.[2,29] Identical cyclic voltammograms were obtained when using Ni anodes in neat aHF and for a solution of dibutylmethylamine in aHF, indicating that the observed anodic process in aHF does not depend on the solute.[24] In fact, the EC_bEC_N mechanism is unreasonable for the fluorination of cationic species and does not account for the substrate fluorination after disconnection of the cell from the power supply (see above).[25,28]

[a] S. Mattsson, Prof. Dr. B. Paulus
Institut für Chemie und Biochemie
Freie Universität Berlin, Arnimallee 22, 14195 Berlin (Germany)
E-mail: stefan.mattsson@fu-berlin.de

[b] G. Senges, Prof. Dr. S. Riedel
Institut für Chemie und Biochemie
Freie Universität Berlin, Fabeckstr. 34–36, 14195 Berlin (Germany)

Supporting information and the ORCID identification number(s) for the author(s) of this article can be found under:
https://doi.org/10.1002/chem.202000881.

© 2020 The Authors. Published by Wiley-VCH Verlag GmbH & Co. KGaA. This is an open access article under the terms of Creative Commons Attribution NonCommercial License, which permits use, distribution and reproduction in any medium, provided the original work is properly cited and is not used for commercial purposes.

Although previous experiments have suggested the formation of active nickel fluorides such as NiF_3 or NiF_4 on the Ni anode,[1,2,24–26] compelling physical evidence is still missing. Additionally, the electrochemical polarization and passivation behavior of nickel in various electrolytes such as (anhydrous) HF,[24,31–34] organic substrates dissolved in HF,[35,36] and HF-containing electrolytes such as NEt_3·3 HF have been intensively investigated in the past.[37] However, a detailed understanding of the ECF process is still missing and the active species in a Simons-type ECF has not yet been clarified.

Well-prepared Ni anodes show an oxidation feature around +4.0 V versus Cu/CuF_2 in HF with low concentrations of water, conductivity additive (e.g., KF) or organic substrate dissolved.[31,34–36] This oxidation potential rises significantly when the water concentration in HF is lowered.[34,36] A reduction peak at +1.0 V versus Cu/CuF_2 was observed and assigned to the reduction of fluorine.[32]

The rapid decomposition of the nickel fluoride film means it is a tough case for characterization by, for example, spectroscopic methods. Quantum-chemical calculations may provide insights to atomistic-scale phenomena for which measurements are either inconceivable or highly challenging. Density functional theory (DFT) is applied widely to surface chemistry problems.[38–47] In recent years, improved methods have emerged for DFT calculations on electrochemical systems with many studies applying the computational hydrogen electrode (CHE) formalism.[48–50] In this study, we set up cyclic voltammetry (CV) experiments and characterize the first oxidation peak in silica, based on DFT models.

Results and Discussion

Cyclic voltammetry measurements

A typical cyclic voltammogram (Figure 1, scan rate 50 mV s^{-1}) of the following system $Ni|NiF_x|HF_l||HF_l|H_{2,g}|Ni$ ($x \geq 2$) contains only one distinct oxidation feature at +3.57 V versus the Pt quasi-reference electrode (QRE), and one reduction feature at +1.42 V, thus indicating two irreversible electrochemical processes. Even at potentials as high as +7.0 V, no additional oxidation peaks are observed.

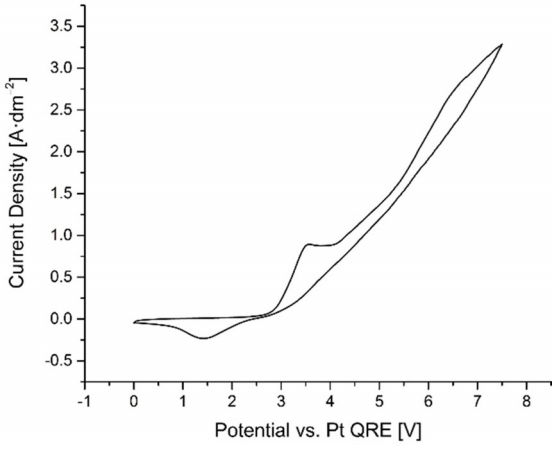

Figure 1. Cyclic voltammograms (scan rate 50 mV s^{-1}) in the potential window from 0.0 V to +7.5 V of the system $Ni|NiF_x|HF_l||HF_l|H_{2,g}|Ni$ ($x \geq 2$) at 0 °C.

Initial formation of a passivation layer on the freshly prepared Ni anode occurs upon application of an oxidizing potential.[1,24,32] It is known that when metallic Ni is exposed to gaseous or liquid HF, the formation of NiF_2 is exergonic.[51] NiF_2 as an electrical insulator is consistent with its proposed role in the passivation of the anode.[52]

NiF_2 surfaces and their potential-dependent fluorination

If NiF_2 is assumed to form a passivating layer on the anode at low voltages, it is conceivable that the first CV peak involves oxidations at various facets of NiF_2 surfaces. In the rutile bulk structure of NiF_2, the Ni^{2+} centers are six-fold coordinated (see Figure S1 in the Supporting Information).

In this project, surface models for a certain Miller index (*h k l*) are constructed according to the two-dimensional slab model where the surface normal points along the [*h k l*] vector. The surface energy, γ, is defined as the energy per surface unit to create a surface cut. The slab model and calculation of γ are described in Section 2 of the Supporting Information.

We consider the low-index surfaces (1 1 0), (1 0 0), (1 0 1), (0 0 1), and (1 1 1). Depending on the amount of F^- ions at the surface (i.e., the surface termination), the oxidation state of surface Ni^{x+} varies between $1 < x < 3$.[53] We first consider $x = 2$, which we refer to as stoichiometric surfaces. Reduced ($x = 1$) and oxidized ($x = 3$) surfaces are referred to as redox surfaces.

Depending on the Miller index, stoichiometric surfaces show lower coordination numbers (CN) at the surface Ni^{2+} centers. In Table 1, we present the stoichiometric surface energies, γ_s, which are calculated with the HSE06 functional. Notably, surfaces with higher surface CNs yield lower surface energies. The surface energies and their ordering are consistent with previous DFT studies on the surface energies of the analogous rutile-type MgF_2 and ZnF_2.[54,55]

Slabs that contain an excess or deficiency of F^- at the surface lead to oxidized or reduced surface Ni centers, respectively.[53] A reservoir of F^- is given in HF. For each additional F^- added to a stoichiometric NiF_2 surface, one H^+ is consumed to form $^1/_2 H_2$. A potential versus the CHE, *V*, is applied a posteri-

Table 1. Surface properties of the NiF_2 surfaces. The surface energy for the stoichiometric (Ni^{2+} at surface) surfaces and surface oxidation potential versus the CHE are calculated with HSE06 in structures optimized with PBE+U. The surface energies depend on the coordination number of the surface Ni^{2+} centers.

	γ_s [J m^{-2}]	Surface CN	$V_{ox,(hkl)}$ [V]
(1 1 0)	0.62	6, 5	+3.21
(1 0 0)	0.69	5	+3.09
(1 0 1)	0.73	5, 5	+3.03
(0 0 1)	0.95	4	+2.71
(1 1 1)	1.08, 1.13[a]	5, 4	+1.74

[a] The (1 1 1) surface has two different terminations, giving stoichiometric surfaces with slightly different γ_s values but the same CNs.

© 2020 The Authors. Published by Wiley-VCH Verlag GmbH & Co. KGaA, Weinheim

ori, which shifts the electrochemical potential of electrons linearly. As half a H_2 molecule is considered to be in equilibrium with H^+ and an electron transferred from the anode, this shifts the chemical potential of H_2 linearly. The two molecules are calculated with DFT methods and expressed as chemical potentials at ambient conditions, through use of thermodynamic tables.[56,57] An advantage here is that entropic effects of the liquid HF need not be considered explicitly, which would drastically increase the complexity of the DFT calculations. On the other hand, as the NiF_2 surfaces are calculated in vacuum, secondary solvent effects at the anode/electrolyte interface are neglected. This topic on its own will be subject to further studies.

The CHE establishes a theoretical reference electrode, which may be directly compared with the Pt quasi-reference electrode (QRE) applied in the CV experiments. This methodology is based solely on thermodynamic equilibria, with the advantage that electron transfers at the electrodes need not to be described explicitly. The approach is closely related to ab initio surface thermodynamics, which is typically employed to study adsorbate coverages as a function of thermodynamic variables such as temperature, partial pressure or, as in this work, the external potential, *V*.[46,47] For a detailed description of the model, we refer to Section 2 of the Supporting Information.

All surface structures are presented in Figure 2. In all oxidized surfaces, F^- is added to a free coordination site of the stoichiometric NiF_2 surface. This increases the surface CN to six (full coverage) for (110), (100), and (101), whereas the (001) surface has the lower CN of five. In all cases, the added F^- is monodentate and its bond length varies between 1.735 and 1.715 Å, which is more consistent with the Ni–F bond length in crystalline NiF_3 (1.88 Å[29,58]) than that of NiF_2 (2.02 Å; Section 1 of the Supporting Information). The very small bond lengths may be explained by the F^- ion exposed to the vacuum. All Ni^{3+} centers (d^7) are characterized by their magnetic moment, which, owing to the high-spin configuration, varies between 2.14 μ_B and 2.18 μ_B. This is in good agreement with the corresponding magnetic moment of 2.30 μ_B in crystalline NiF_3, which was calculated with HSE06.[58]

For the oxidized (111) surface, the added F^- bridges between two surface Ni centers leading to an increase in CNs from five and four to six and five. The formed Ni^{3+} center is five-fold coordinated and situated in a pocket at the surface. The free coordination site is facing directly away from the surface. Interestingly, this leads to a low-spin configuration with a magnetic moment of 1.01 μ_B. The unpaired electron occupies a d_{z^2} orbital, which favorably points directly away from the ligands, at the free coordination site.

Reduced surfaces have low surface CNs and, to compensate for this, the surfaces are strongly contracted. The surface Ni^+ (d^9) magnetic moments vary between 0.97 μ_B and 1.01 μ_B for all reduced surfaces except for (110) at 1.25 μ_B, where the hybridization with F^- ions is greater.

Figure 3 shows the calculated γ for all surfaces as a function of *V* versus the CHE. The linear relationship from the CHE formalism allows for easy interpretation of the data. For a given Miller index, the oxidation state with the lowest γ is the most stable. Hence, for the Miller index, there is a crossing point at sufficiently high *V*, where the third oxidation state is thermodynamically favored. Because we study an anodic process, we are not interested in negative potentials. Furthermore, if γ becomes negative at some *V*, the model is no longer valid. This implies that the surface is more stable than its underlying crystal and suggests a scenario in which, at high *V*, the crystal may start deforming to allow further oxidation at deeper layers below the NiF_2 surface.

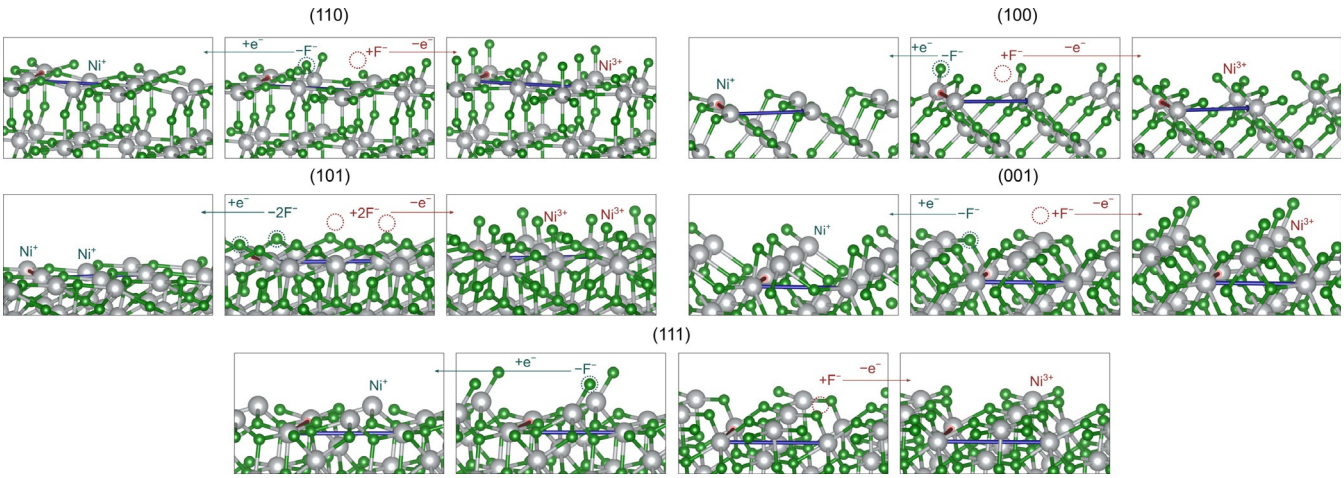

Figure 2. Structures of the considered NiF_2 surfaces as optimized with PBE + U. For each Miller index, the stoichiometric surfaces are drawn in the middle. Dashed circles indicate where an F^- is removed in the reduction (blue) or an empty coordination site too which F^- is added in the oxidation (red). Blue and red arrows point towards the reduced and oxidized surfaces, respectively. The Ni centers of the changed oxidation state are labeled with the same colors. For the (111) surface, both stoichiometric terminations are shown, where one is more easily reduced whereas the other is more easily oxidized. The transferred electrons are considered in the energy of half a H_2 molecule.

© 2020 The Authors. Published by Wiley-VCH Verlag GmbH & Co. KGaA, Weinheim

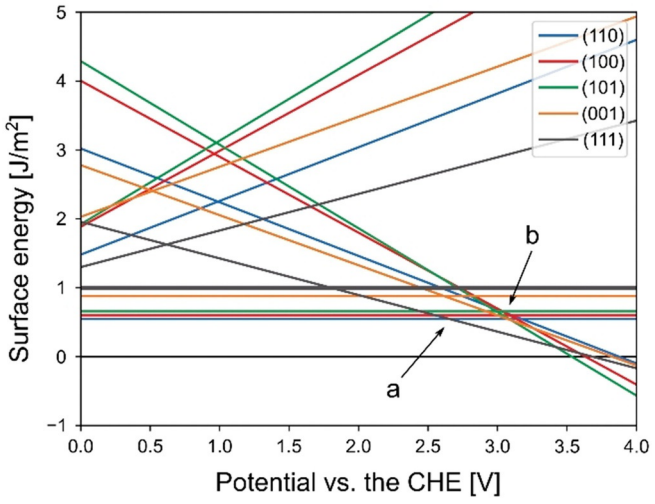

Figure 3. Calculated potential-dependent surface energies of NiF_2. Lines with a slope of 0 correspond to stoichiometric surfaces. Negative slopes correspond to the oxidation to Ni^{3+} at the surface whereas positive slopes correspond to the reduction to Ni^{+}. Here, a (+2.7 V) marks the crossing point where the oxidized (111) surface becomes the most stable. At b (+3.1 V), all oxidized surfaces become more stable than the stoichiometric ones. The structures are relaxed with PBE+U and the energies calculated with HSE06.

Discussion

We now compare our experimental CV with the calculated potential-dependent surface stabilities. As the stoichiometric surfaces of NiF_2 do not involve any redox processes, the surface energies are independent of the potential. At low *V*, the calculated stoichiometric surfaces dominate stability-wise (Figure 3), which is reflected in the absence of current between 0 and +3 V (vs. QRE) in Figure 1. Owing to the lower surface energies, the stoichiometric (1 1 0), (1 0 0), and (1 0 1) surfaces are expected to occur in this potential range.

At higher *V*, calculated oxidized surfaces become more stable than stoichiometric surfaces. This point, $V_{ox,(hkl)}$, is specific for each Miller index and the values are listed in Table 1. We find that there is a clear linear relationship between $V_{ox,(hkl)}$ and γ_s for all surfaces except (1 1 1) (Figure S4 in the Supporting Information). The linear relationship intuitively means that the less stable stoichiometric surface cuts are more easily fluorinated.

Additionally, (111) shows a $V_{ox,(hkl)}$ lower than the linear fit of the four other surfaces. The stabilizing pocket for the Ni^{3+} centers clearly makes this surface an outlier. In fact, at around +2.7 V (vs. CHE), it becomes more stable than the stoichiometric surfaces. However, the stoichiometric (111) surface is unlikely to appear in the parent NiF_2 film owing to its high surface energy.

At +3.1 V (vs. CHE), the calculated oxidized surfaces become more stable than all stoichiometric surfaces. At this point our model suggests that current will flow through the cell as the first Ni^{2+} layer of the low-energy stoichiometric surfaces is oxidized. The calculated results match our measured onset potential well. Therefore, the oxidation peak at the potential of +3.57 V (vs. QRE) is assigned as the oxidation of Ni^{2+} to Ni^{3+}. It must be noted that the assignment ignores the possible occurrence of a mixed valence state of the type $Ni^{2+}[Ni^{4+}F_6]$[59,60] or $Ni^{2+}[Ni^{3+}F_5]$.[61] Furthermore, more complicated amorphous structures are possible for the film.

The coherence between experiment and theory suggests that the passivation layer is NiF_2, which is assumed to be subsequently oxidized to a higher NiF_x ($x>2$) species at sufficiently high potential.[1] The mechanism of the subsequent fluorination of organic substrates may involve formal Ni^{3+} or Ni^{4+} fluorides, but alternative pathways based on fluorine radicals or adsorbed fluorine are still conceivable if the oxidized anodic film (NiF_3) loses F_2 during cathodic stripping.[31]

Conclusion

We have considered the activation of Ni anodes in aHF, which is a key step in the Simons-type ECF reaction. The anodic CV peak at +3.57 V (vs. QRE) is likely the oxidation of Ni^{2+} to Ni^{3+}. Results from previous experiments have proven that NiF_2 easily forms at Ni/HF interfaces. With the assumption that an insulating NiF_2 film covers the anode until approximately +3 V, we have calculated the oxidation potential of NiF_2. This is done on the basis of DFT calculations and thermodynamic arguments, through consideration of various NiF_2 surface motifs. The measured and calculated potentials agree well, and we assign the anodic peak to the oxidation of Ni^{2+} to Ni^{3+}.

Experimental Section

Cyclic voltammetry measurements

The disc electrodes employed for the CV measurements consisted of Ni (99.98%, ChemPur) or Pt (99.99%, ChemPur) wire of 1 mm in diameter with a PFA (perfluoroalkoxy) coating. Prior to use, the electrodes were sanded with 800-grit sandpaper to a smooth finish, immersed in nitric acid (65%) for 1 min, immediately washed with purified water afterwards, and dried on air. A Bio Logic Science Instruments Pvt. Ltd. SAS model SP-300 potentiostat and the software EC-Lab®[50] were used for the CV measurements. Hydrogen fluoride was obtained from GHC Gerling Holz & Co. Handels GmbH and was used as received. For safety reasons, the required amount of hydrogen fluoride (approximately 10 mL) was condensed in a PFA reservoir at −196 °C by using a stainless-steel high vacuum line and consequentially pumped into the open electrochemical cell with a slight overpressure of argon via a PFA tube at −80 °C. The temperature of the electrolyte was kept at 0 °C by using an ice/water bath during the electrochemical measurements. To oxidize residual water in the electrolyte, the freshly polished electrodes were pre-conditioned by cycling between 0.0 V and 6.0 V versus Pt QRE until no oxidation peak at 1.0 V versus Pt QRE was observed (typically three cycles).

Computational details

All calculations were performed by using the spin-polarized periodic density functional theory (DFT), as implemented in the plane-wave-based Vienna ab-initio simulation package (VASP) version 5.4.1.[62–64] Core electrons are described by using the projector-augmented-wave method with the standard GGA pseudopotentials provided by VASP.[65] Plane-waves of kinetic energies up to 700 eV

© 2020 The Authors. Published by Wiley-VCH Verlag GmbH & Co. KGaA, Weinheim

are included as the basis set. The first Brillouin zone of bulk NiF_2 was sampled with a Monkhorst–Pack k-point grid of $8\times8\times8$.[66] For slab calculations, k-point grids of $8\times8\times1$ were used where the last number refers to the non-periodic direction. The self-consistent field method convergence criterion was set to 0.1 meV. Gaussian smearing was employed with a σ factor of 0.1 eV. With the specified plane wave cutoff, k-point sampling and smearing factor, the absolute energy per atom was converged within 1 meV per formula unit NiF_2 in the bulk unit cell.

Three different exchange-correlation functionals were used for calculation of the bulk properties: the GGA implementation according to Perdew–Burke–Ernzerhof (PBE),[67] the same functional with an added Hubbard-type U correction term to account for localized d electrons (PBE+U)[68] and the range-separated hybrid functional HSE06.[69] The Hubbard U parameter for Ni, 5.3 eV, was taken from a previous study on the electronic properties of NiO.[70] The PBE+U functional is regarded as a more affordable alternative to hybrid functionals, while describing the electronic structure with comparable accuracy.[71]

For bulk NiF_2, structure optimizations were performed simultaneously for the lattice parameters and internal coordinates until the ionic forces were no larger than 0.01 eV $Å^{-1}$. Band gaps were calculated by using the three functionals with the HSE06 band gap serving as a benchmark value. All bulk results are presented in Section 1 of the Supporting Information.

For the slabs, structure optimizations were performed only for internal coordinates and with the PBE+U functional. HSE06 surface energies were calculated by using the structures optimized with PBE+U. Cell parameters *a* and *b* were picked from the bulk structure and frozen so that they matched the underlying bulk structure. The third vector points towards [*h k l*] (perpendicular to the slab). A vacuum of around 20 Å was added in the non-periodic direction for all slab calculations to avoid artificial interactions between slabs.

For the CHE calculations, the H_2 and HF molecules were structurally optimized, and the energies calculated with the HSE06 functional. To avoid interaction between molecules in different cell images, a vacuum of 20 Å was added in all directions. Thermodynamic data for extrapolation of the chemical potential to ambient conditions was taken from the NIST and CODATA databases.[56,57] For redox surfaces, the surface energies were extrapolated to 298 K. The pressure was taken as 1 bar for H_2 and 1.973 bar (the vapor pressure at 298 K) for HF.[56] For the chemical activity of H^+, the Hammett acidity function of HF was taken as $H_0 = -11$.[72]

Bader charges were calculated by using an external program developed by Henkelman et al.[73] The magnetic moment (in units of the Bohr magneton) of an atom was calculated from the difference in spin-up and spin-down density within the Bader volume of the atom.

All structures were visualized by using VESTA 3.4.4.[74] The structures used are included in the Supporting Information.

Acknowledgments

We gratefully acknowledge the funding of our work from the German Research Foundation (DFG) through the collaborative research center SFB 1349 "Fluorine-Specific Interactions", project ID 387284271 (Gefördert durch die Deutsche Forschungsgemeinschaft (DFG), Projektnummer 387284271, SFB 1349). We also thank the Network of High-Performance Computers in Northern Germany (HLRN) for computational resources within the research project bec00154. We also express our gratitude towards the Central Computing Services of the Freie Universität Berlin (ZEDAT) for maintenance of our computer facilities. We thank Dr. Nikolai Ignat'ev, Dr. Simon Steinhauer, and Dr. Helmut Beckers for useful discussions. We also acknowledge Hannah Eyre for careful proofreading of the manuscript. Open access funding enabled and organized by Projekt DEAL.

Conflict of interest

The authors declare no conflict of interest.

Keywords: cyclic voltammetry · electrocatalysis · fluorination · nickel fluorides · quantum-chemical calculations

[1] N. V. Ignat'ev in *Modern Synthesis Processes and Reactivity of Fluorinated Compounds* (Eds.: H. Groult, F. Leroux, A. Tressaud), Elsevier, Oxford, **2017**, pp. 71–123.
[2] N. V. Ignat'ev, U. Welz-Biermann, U. Heider, A. Kucheryna, S. von Ahsen, W. Habel, P. Sartori, H. Willner, *J. Fluorine Chem.* **2003**, *124*, 21–37.
[3] Y. W. Alsmeyer, W. V. Childs, R. M. Flynn, G. G. I. Moore, J. C. Smeltzer in *Organofluorine Chemistry* (Eds.: R. E. Banks, B. E. Smart, J. C. Tatlow), Plenum Press, New York, **1994**, pp. 121–143.
[4] P. Sartori, N. Ignat'ev, *J. Fluorine Chem.* **1998**, *87*, 157–162.
[5] *Results of the 2006 survey on production and use of PFOS, PFAS, PFOA, PFCA, their related substances and products/mixtures containing these substances*, OECD, Paris.
[6] *Hazard assessment of perfluorooctance sulfonate (PFOS) and its salts*, OECD, Paris, **2002**.
[7] *Environmental and health assessment of perfluorooctane sulfonic acid and its salts*, 3M, Maplewood, MN, **2003**.
[8] M. Schmeisser, P. Sartori, *Chem. Ing. Tech.* **1964**, *36*, 9–14.
[9] W. H. Pearlson, U.S. Patent 3274081 (to 3M Co.).
[10] W. H. Pearlson, *J. Fluorine Chem.* **1986**, *32*, 29–40.
[11] G. G. Totir, G. S. Chottiner, C. L. Gross, D. A. Scherson, *J. Electrochem. Soc.* **2001**, *148*, E262–E266.
[12] J. H. Simons, U.S. Patent 2519983 (to 3M Co.).
[13] J. H. Simons, *J. Electrochem. Soc.* **1949**, *95*, 47–52.
[14] J. H. Simons, H. T. Francis, J. A. Hogg, *J. Electrochem. Soc.* **1949**, *95*, 53–55.
[15] J. H. Simons, W. J. Harland, *J. Electrochem. Soc.* **1949**, *95*, 55–59.
[16] J. H. Simons, W. H. Pearlson, T. J. Brice, W. A. Wilson, R. D. Dresdner, *J. Electrochem. Soc.* **1949**, *95*, 59–64.
[17] J. H. Simons, R. D. Dresdner, *J. Electrochem. Soc.* **1949**, *95*, 64–67.
[18] L. Conte, G. P. Gambaretto, *J. Fluorine Chem.* **2004**, *125*, 139–144.
[19] G. P. Gambaretto, M. Napoli, L. Conte, A. Scipioni, R. Armelli, *J. Fluorine Chem.* **1985**, *27*, 149–155.
[20] J. Burdon, I. W. Parsons, J. C. Tatlow, *Tetrahedron* **1972**, *28*, 43–52.
[21] H. Meinert, H. Schmidt, *Angew. Chem.* **1960**, *72*, 109–110.
[22] I. N. Rozhkov, *Russ. Chem. Rev.* **1976**, *45*, 615–629.
[23] H. Meinert, J. Mader, W. Röhlke, U. Thewalt, T. Debaerdemaeker, *J. Fluorine Chem.* **1994**, *67*, 235–240.
[24] A. Dimitrov, St. Rüdiger, N. V. Ignat'ev, S. Datcenko, *J. Fluorine Chem.* **1990**, *50*, 197–205.
[25] A. Dimitrov, D. Pfeifer, U. Jonethal, St. Rüdiger, K. Seppelt, *J. Fluorine Chem.* **1997**, *82*, 143–150.
[26] N. Ignat'ev, P. Sartori, *J. Fluorine Chem.* **2000**, *103*, 57–61.
[27] U. Groß, St. Rüdiger, A. Dimitrov, *J. Fluorine Chem.* **1996**, *76*, 139–144.
[28] P. Sartori, N. Ignat'ev, S. Datsenko, *J. Fluorine Chem.* **1995**, *75*, 157–161.
[29] B. Žemva, K. Lutar, L. Chacón, M. Fele-Beuermann, J. Allman, C. Shen, N. Bartlett, *J. Am. Chem. Soc.* **1995**, *117*, 10025–10034.
[30] J. M. Whalen, L. C. Chacón, N. Bartlett in *Electrochemistry in the Preparation of Fluorine and its Compounds, Proceedings, Vols. 97–15* (Eds.: W. V. Childs, T. Fuchigami), The Electrochemical Society, Pennington, **1997**, pp. 1–12.
[31] N. Watanabe, *J. Fluorine Chem.* **1983**, *22*, 205–230.

 © 2020 The Authors. Published by Wiley-VCH Verlag GmbH & Co. KGaA, Weinheim

[32] N. Hackerman, E. S. Snavely, Jr., L. D. Fiel, *Electrochim. Acta* **1967**, *12*, 535 – 551.
[33] J. A. Donohue, A. Zletz, R. J. Flannery, *J. Electrochem. Soc.* **1968**, *115*, 1042 – 1045.
[34] N. Watanabe, M. Haruta, *Electrochim. Acta* **1980**, *25*, 461 – 464.
[35] B. Chang, N. Watanabe, K. Nakanishi, *Electrochim. Acta* **1972**, *17*, 1317 – 1331.
[36] B. Chang, H. Yanase, K. Nakanishi, N. Watanabe, *Electrochim. Acta* **1971**, *16*, 1179 – 1196.
[37] S. Sathyamoorthi, D. Velayutham, V. Suryanarayanan, M. Noel, *Electrochim. Acta* **2011**, *56*, 7012 – 7021.
[38] W. Yu, M. D. Porosoff, J. G. Chen, *Chem. Rev.* **2012**, *112*, 5780 – 5817.
[39] D. Vogel, C. Spiel, Y. Suchorski, A. Trinchero, R. Schlögl, H. Grönbeck, G. Rupprechter, *Angew. Chem. Int. Ed.* **2012**, *51*, 10041 – 10044; *Angew. Chem.* **2012**, *124*, 10185 – 10189.
[40] U. Bauer, S. Mohr, T. Döpper, P. Bachmann, F. Späth, F. Düll, M. Schwarz, O. Brummel, L. Fromm, U. Pinkert, A. Görling, A. Hirsch, J. Bachmann, H.-P. Steinrück, J. Libuda, C. Papp, *Chem. Eur. J.* **2017**, *23*, 1613 – 1622.
[41] J. Schumann, A. J. Medford, J. S. Yoo, Z.-J. Zhao, P. Bothra, A. Cao, F. Studt, F. Abild-Pedersen, J. K. Nørskov, *ACS Catal.* **2018**, *8*, 3447 – 3453.
[42] A. Travert, H. Nakamura, R. A. van Santen, S. Cristol, J.-F. Paul, E. Payen, *J. Am. Chem. Soc.* **2002**, *124*, 7084 – 7095.
[43] M. Witko, R. Tokarz-Sobieraj, *Catal. Today* **2004**, *91 – 92*, 171 – 176.
[44] C. Arrouvel, M. Digne, M. Breysse, H. Toulhoat, P. Raybaud, *J. Catal.* **2004**, *222*, 152 – 166.
[45] M. Boronat, P. Concepción, A. Corma, *J. Phys. Chem. C* **2009**, *113*, 16772 – 16784.
[46] M. Habgood, N. Harrison, *Surf. Sci.* **2008**, *602*, 1072 – 1079.
[47] C. L. Bailey, S. Mukhopadhyay, A. Wander, B. G. Searle, N. Harrison, *J. Phys. Chem. C* **2009**, *113*, 4976 – 4983.
[48] F. Calle-Vallejo, M. T. M. Koper, *Electrochim. Acta* **2012**, *84*, 3 – 11.
[49] J. K. Nørskov, J. Rossmeisl, A. Logadottir, L. Lindqvist, J. R. Kitchin, T. Bligaard, H. Jónsson, *J. Phys. Chem. B* **2004**, *108*, 17886 – 17892.
[50] J. Rossmeisl, J. K. Nørskov, C. D. Taylor, M. J. Janik, M. Neurock, *J. Phys. Chem. B* **2006**, *110*, 21833 – 21839.
[51] G. G. Totir, G. S. Chottiner, C. L. Gross, W. Ves Childs, D. A. Scherson, *J. Electrochem. Soc.* **2000**, *147*, 4212 – 4216.
[52] P. Olalde-Velasco, J. Jiménez-Mier, J. D. Denlinger, Z. Hussain, W. L. Yang, *Phys. Rev. B.* **2011**, *83*, 241102.
[53] In periodic calculations, the unit cell must be charge-neutral to avoid a build-up of infinite charge. In practice, when, for example, adding an "F^-" to a stoichiometric surface, an F atom is added upon which one electron gets transferred from the Ni^{2+} center to which it binds.
[54] Z. Huesges, C. Müller, B. Paulus, C. Hough, N. Harrison, E. Kemnitz, *Surf. Sci.* **2013**, *609*, 73 – 77.
[55] Z. Kaawar, B. Paulus, *AIP Conf. Proc.* **2015**, *1702*, 020051.
[56] a) https://webbook.nist.gov/cgi/cbook.cgi?Name=h2&cTG=on, accessed December 18, **2019**; b) https://webbook.nist.gov/cgi/cbook.cgi?ID=C7664393&Mask=1, accessed December 18, **2019**.
[57] http://www.codata.info/resources/databases/key1.html, accessed December 18, **2019**.
[58] S. Mattsson, B. Paulus, *J. Comput. Chem.* **2019**, *40*, 1190 – 1197.
[59] A. L. Hector, E. G. Hope, W. Levason, M. T. Weller, *Z. Anorg. Allg. Chem.* **1998**, *624*, 1982 – 1988.
[60] C. Shen, L. C. Chacón, N. Rosov, S. H. Elder, J. C. Allman, N. Bartlett, *C. R. Acad. Sci. Paris* **1999**, 2, Série II, c, 557 – 563.
[61] M. Tramšek, B. Žemva, *Acta Chim. Slov.* **2002**, *49*, 209 – 220.
[62] G. Kresse, J. Hafner, *Phys. Rev. B* **1993**, *47*, 558 – 561.
[63] G. Kresse, J. Hafner, *Phys. Rev. B* **1994**, *49*, 14251 – 14269.
[64] G. Kresse, J. Furthmüller, *Comput. Mater. Sci.* **1996**, *6*, 15 – 50.
[65] P. E. Blöchl, *Phys. Rev. B* **1994**, *50*, 17953 – 17979.
[66] H. J. Monkhorst, J. D. Pack, *Phys. Rev. B* **1976**, *13*, 5188 – 5192.
[67] J. P. Perdew, K. Burke, M. Ernzerhof, *Phys. Rev. Lett.* **1996**, *77*, 3865 – 3868.
[68] S. L. Dudarev, G. A. Botton, S. Y. Savrasov, C. J. Humphreys, A. P. Sutton, *Phys. Rev. B* **1998**, *57*, 1505 – 1509.
[69] A. V. Krukau, O. A. Vydrov, A. F. Izmaylov, G. E. Scuseria, *J. Chem. Phys.* **2006**, *125*, 224106.
[70] A. Rohrbach, J. Hafner, G. Kresse, *Phys. Rev. B* **2004**, *69*, 075413.
[71] P. Verma, D. G. Truhlar, *Theor. Chem. Acc.* **2016**, *135*, 182.
[72] F. A. Cotton, G. Wilkinson, *Advanced Inorganic Chemistry, Vol. 4*, Wiley, New York, **1980**, p. 238.
[73] G. Henkelman, A. Arnaldsson, H. Jónsson, *J. Molec. Graphics* **1996**, *14*, 33 – 38.
[74] K. Momma, F. Izumi, *J. Appl. Crystallogr.* **2011**, *44*, 1272 – 1276.

Manuscript received: February 18, 2020
Accepted manuscript online: May 7, 2020
Version of record online: July 21, 2020

 © 2020 The Authors. Published by Wiley-VCH Verlag GmbH & Co. KGaA, Weinheim